crystals

MDPI

Article

Magnetoelectric Properties of Aurivillius-Layered Perovskites

Vadla Veenachary [1], Eskilla Venkata Ramana[2,*], Simhachalam Narendrababu[1], Venkata Sreenivas Puli[3], Sujoy Saha[4], Gopalan Srinivasan[4], and G. Prasad [1] and N. V. Prasad[1,*]

[1] Materials Research Laboratory, Department of Physics, Osmania University, Hyderabad, 500 013 India; veenachary1@gmail.com. (V.V), narendraphysics@gmail.com (S.N.B.);
[2] I3N-Aveiro, Department of Physics, University of Aveiro, Aveiro-3810 193, Portugal;
[3] Smart Nanomaterials Solutions, Orlando, FL, 32707, USA; pvsri123@gmail.com
[4] Physics Department, Oakland University, Rochester, Michigan, USA; srinivas@oakland.edu
*Correspondence: nvp1969@rediffmail.com, raman.venkata@ua.pt

Abstract: In the present work, we have synthesized rare-earth ions (RE=Dy, Sm, La) modified $Bi_{4-x}RE_xTi_2Fe_{0.7}Co_{0.3}O_{12-\delta}$ (DBTFC, SBTFC, and LBTFC) multiferroic compounds by conventional solid-state route. The analysis of x-ray diffraction by Rietveld refinement confirmed the formation of polycrystalline orthorhombic phase. The morphological features reveal non-uniform, randomly oriented plate-like grain structure. The spectral features from Raman data suggests the formation of Aurivillius phases whose modes match well with orthorhombic structure. Dielectric studies and impedance measurements were carried out. Asymmetric complex impedance spectra suggest the relaxation of charge carriers belonging to the non-Debye type and controlled by a thermally activated process. Temperature-dependent ac-conductivity data has shown a change of slope in the vicinity of phase transition temperature of both magnetic and electrical coupling nature. Based on the universal law, and its exponent nature, one can attribute that the conduction process is governed by a small polaron hopping process and significant distortion of TiO_6 octahedra. The effect of rare earth doping in the A-site and Fe^{2+} and Co^{2+} ion concentration at the B-site has shown saturated magnetic hysteresis loop loops indicating a competitive interaction of both ferroelectric and canted antiferromagnetic spins. The magnetic order in the samples is attributed to double-exchange interactions between adjacent Fe^{3+} - O - Fe^{3+}, $Co^{2+/3+}$ - O - $Co^{3+/2+}$, and $Co^{2+/3+}$ - O - Fe^{3+} ions or DM interactions among magnetic ions in the adjacent sub-lattices. As a result, enhanced magnetoelectric coefficients of 42.4 mV/cm-Oe, 30.3 mV/cm-Oe, and 21.6 mV/cm-Oe for DBTFC, LBTFC, and SBTFC respectively at lower magnetic fields, below 3 kOe. The strong coupling of the Aurivillius multiferroic compounds observed in this study is beneficial to future multiferroic one-to-many applications.

Keywords: Mmultiferroic; Aurivillius; Impedance spectra; Magnetoelectric; Dielectric studies, Magnetic studies; Structural studies.

Citation: To be added by editorial staff during production.

Academic Editor: Firstname Lastname

Received: date
Revised: date
Accepted: date
Published: date

1. Introduction

Multiferroic compounds are a fascinating type of materials that have garnered remarkable attention in the realm of materials science. Multiferroics exhibit two or more orders of ferroelectric (FE), ferro-elastic, and magnetic (ferromagnetism (FM)/anti-ferromagnetism (AFM)) orders in the single phase. The present Aurivillius phase materials have shown their potential usage in many novel applications, like memory storage devices, sensors, transducers, and actuators. Multiferroics are promising materials, drawing researchers, due to their potential applications that exploit the coupling between ferroelectric and magnetic orders [1,2]. The most fascinating prospect of research on these materials is tuning the electric dipoles by applying magnetic fields under superimposed small ac-magnetic fields [3–7]. The coupling between ferroelectric (FE) and ferromagnetic

(FM) order makes it easier and faster to write or read a data bit in memory devices [2,8]. This could lead to the development of magnetoelectric materials owing to their speed read/write operations. However, in reality, very few room-temperature ME compounds have been reported, due to the mutual exclusion nature of FM and FE in single-phase compounds. The ferroelectricity is attributed to empty d-orbitals, while partially or half-filled d-orbitals show for magnetic nature [9]. In the path of searching for single-phase multiferroic compounds, Aurivillius phase multiferroics are a class of bismuth layer structured compounds that have been extensively investigated for their flexibility and tunable nature of ferroelectric and magnetic properties at the quantum state [10–17].

The general formula of Aurivillius phase compounds can be expressed as $(Bi_2O_2)^{2+}(A_{m-1}B_mO_{3n+1})^{2-}$, where m represents the number of perovskites ($A_{m-1}B_mO_{3n+1}$), which are sandwiched between fluorite like $(Bi_2O_2)^{2+}$ layers. Here A is the cuboctahedra site, which can be substituted by mono-, di-, or tri-valent elements and B is the octahedral site (BO_6), which can be substituted by di-, tri-, tetra-, or pentavalent elements[18]. The Aurivillius phase compounds were found to be familiar for their ferroelectric/magnetoelectric behaviour, high transition temperatures, and strong anisotropic nature of spontaneous polarization [19]. Rare earth-modified A-site Aurivillius phases were studied to explore the change in structural and ferroelectric properties [20]. These materials are well-suitable for non-volatile memory devices due to their highly fatigue-free nature. Recently many Aurivillius phase compounds have shown room temperature magnetoelectric output when Fe/Co/Ni were substituted in the B-site of the chemical formula. However, the nature and origin of the combined ferroelectric and magnetic nature and its coupling are still under discussion. Therefore, a strategic way is required in choosing magnetic ions, which triggers the enhanced magnetoelectric output in the materials. It is a known fact that the multiferroic properties of materials can be altered by altering the concentration of magnetic ions in the B-site of Aurivillius phases. From previous literature, iron-doped Aurivillius phase compounds show a strong multiferroic behaviour at room temperature [12, 21]. These multiferroic materials are also known expressed as $Bi_{m+1}Fe_{m-3}Ti_3O_{3m+3}$ (BFTO-m). More interestingly, the key factors of the Aurivillius phase materials are: (i) the origin of ferroelectricity is a combination of oxygen octahedral rotation and polar distortion; (ii) different numbers of layers in perovskite plates show significant differences in physical and structural properties.

In the last decade, much research has been focused on different layer compounds, such as $Bi_5FeTi_3O_{15}$, $Bi_6Fe_2Ti_3O_{18}$, $Bi_7Fe_3Ti_3O_{21}$, etc.,[22–28]. The reported study on the Aurivillius family embodies two main aspects: (i) the tailoring of ions on the A-sites and of magnetic ionic incorporation on B-sites enhance the multiferroic performance, (ii) ceramics, thin films, single crystals, and intergrowth controllable synthetic growth route techniques were adopted to understand structure-property relationship[29–36].

The three-layer structure bismuth titanate ($Bi_4Ti_3O_{12}$ – BIT) has attracted researchers due to its high transition temperature (above 600^0C), low processing temperature compared to higher layer structure compounds, and its anisotropic behaviour of ferroelectricity[37–41]. However, these compounds possess high conductivity due to the volatile nature of bismuth at higher temperatures. The volatile nature of bismuth creates bismuth vacancies and is accompanied by oxygen vacancies. This intern results in leakage currents, which demote the ferroelectric nature [42–45]. This kind of limitation can be controlled by substituting rare earth (RE) ions in the A-site of BIT compounds [13, 46, 47]. A noteworthy observation by Lu et al. is that Fe-doped BIT ceramics exhibit room-temperature weak ferromagnetic behaviour [48]. Shigyo et al. reported that the La, Nd, and Sm doped BIT samples show improved magnetic and ferroelectric properties by controlling oxygen vacancies [49]. According to Paul et al., the compound, $Bi_{4-x}Sm_xTi_{3-x}Co_xO_{12-\delta}$ at x=0.07 has shown the coefficient of magnetoelectric (ME) coupling is about α = 0.65mVcm^{-1}[50]. In recent studies, Zhonghui Yu et al. have reported that the ME coefficient of 31.58 mVcm^{-1}Oe^{-1} for $Bi_4LaTi_3Co_{0.3}Fe_{0.7}O_{15}$ ceramics [51]. Aurivillius phases having antiferromagnetic order or weak magnetic order, restricts for their practical applications. And the

substitution of magnetic ions for B-sites deteriorates the ferroelectric nature on account of defects [52–54]. These defects can be controlled by substituting RE ions for A- sites of Aurivillius phases. It should be remembered that the stoichiometry and synthesis conditions play a vital role in optimizing the properties of the compounds.

In the present work, we have prepared RE (Dy, Sm, La) ion-doped $Bi_4Ti_2Fe_{0.7}Co_{0.3}O_{12-\delta}$ (DBTFC, SBTFC, and LBTFC respectively) ceramics. Electrical, magnetic, and magnetoelectric measurements were made on the above said samples. The major endeavour of the present work is to diminish the leakage current by introducing RE ions in the A-sites of perovskites and enhancing the magnetoelectric coupling. The dispersion in ac-conductivity and relaxations on similar samples and relaxations in the low-frequency range above 200ºC were explained in terms of Maxwell-Wagner relaxation and multiple relaxations (non-Debye type). The presence of a small polaron conduction mechanism plays a vital role. The dielectric relaxations observed near 200ºC were attributed to the change hopping of Ti^{3+} to Ti^{4+}/ Fe^{2+} to Fe^{3+} ions. The substitution of low-concentration rare earth ions enhances the dielectric properties on the other hand it shows contradicting results. Apart from the above pioneering aspects, understanding structural evolution is an interesting task in Aurivillius phase compounds. Systematic studies on X-ray, Raman, and impedance spectroscopic studies confirm the inherited magnetoelectric properties. Queerly, the Dy-doped $Bi_4Ti_2Fe_{0.7}Co_{0.3}O_{12-\delta}$ (DBTFC) sample has shown a higher ME coefficient of ~ 42.4 mV/cm-Oe at room temperature, at lower fields. Such systematic studies have hitherto not been reported so far.

2. Materials and Methods

AAurivillius multiferroic ceramics, Dy, Sm, and La (ionic radii 1.027, 1.079, and 1.16 Aº respectively) rare earth ion doped $Bi_4Ti_2Fe_{0.7}Co_{0.3}O_{12-\delta}$ compounds are synthesized by conventional solid-state reaction method. Priory, Bi_2O_2, Sm_2O_2, Dy_2O_3, La_2O_3, TiO_2, Fe_2O_3, and Co_3O_4 with more than 99.9% purity, are taken in stoichiometric ratio to synthesize three-layered $Bi_3RETi2Fe0_{.7}Co_{0.3}O_{12-\delta}$. The mixed powders are grounded in the planetary ball mill for 24 hours and subsequently, the mixed powders are calcinated at 850^{0}C for 4 hours. The calcined powder was again grounded for 6 hours by agate motor and pestle. The calcined powder was investigated for phase analysis employing X-ray diffraction measurements. The powder was made into circular pellets with a thickness of around 1mm and a diameter of 10mm by using a uni-axial hydraulic pressing machine. The green pellets are sintered at 900^{0}C for 4 hours to attain higher density. The RE (Dy, Sm, and La) ion-doped $Bi_4Ti_2Fe_{0.7}Co_{0.3}O_{12-\delta}$ compounds are named as DBTFC, SBTFC, and LBTFC respectively.

Phase conformation of all the samples was done by Powder X-ray diffraction using a PAN analytic X'Pert diffractometer. The Rietveld refinement is also done for all samples by using Full-Prof Suit software. The phase of all samples is well matched with standard three-layered compounds of XRD data (ICSD#87077). To study surface morphology and elemental analysis (Energy Dispersive X-ray spectroscopy (EDAX)) the samples are alysed by using ZEISS- EVO185 SEM instrument. ImageJ software is used to calculate the average grain size on the sintered pellets by employing histograms with Gaussian distribution. Raman spectroscopic studies were also employed by using a Jobin Yvon spectrometer with a 532nm excitation laser beam. The magnetization vs external magnetic field studies were carried out using a vibrating sample magnetometer (VSM). Magnetoelectric studies are measured using a micro-measurement Group Strain Indicator, Model 3800, and series WK strain gauge. The samples are electrically and magnetically polled, before performing ME measurements. The ferroelectric studies are measured under various driving voltages using a P-E loop tracer. Before carrying out electrical measurements, the pellets are polled under an electric field. Prior to the magnetoelectric measurements, the samples were polled by subjecting the cylindrical pellets to electric and magnetic fields separately. Samples were polled by placing them in the silicon oil bath, heated up to 120°C, and cooled in

the presence of the field. Magnetic polling was done by placing the samples in magnetic fields at 5 kOe at room temperature (RT).

3. Results and discussions

3.1 Powder X-ray diffraction and morphological studies

The powder X-ray diffraction patterns of DBTFC, SBTFC, and LBTFC compounds were obtained in the range of 20^0 - 80^0 at room temperature. The diffraction peaks of the compounds are in good agreement with the standard XRD pattern of $Bi_4Ti_3O_{12}$ (ICSD#87077) with space group *Fmmm* as shown in Fig 1(a-c)[55,56]. The XRD data was fitted into Rietveld refinement with Full-Prof software. The refinement analysis shows

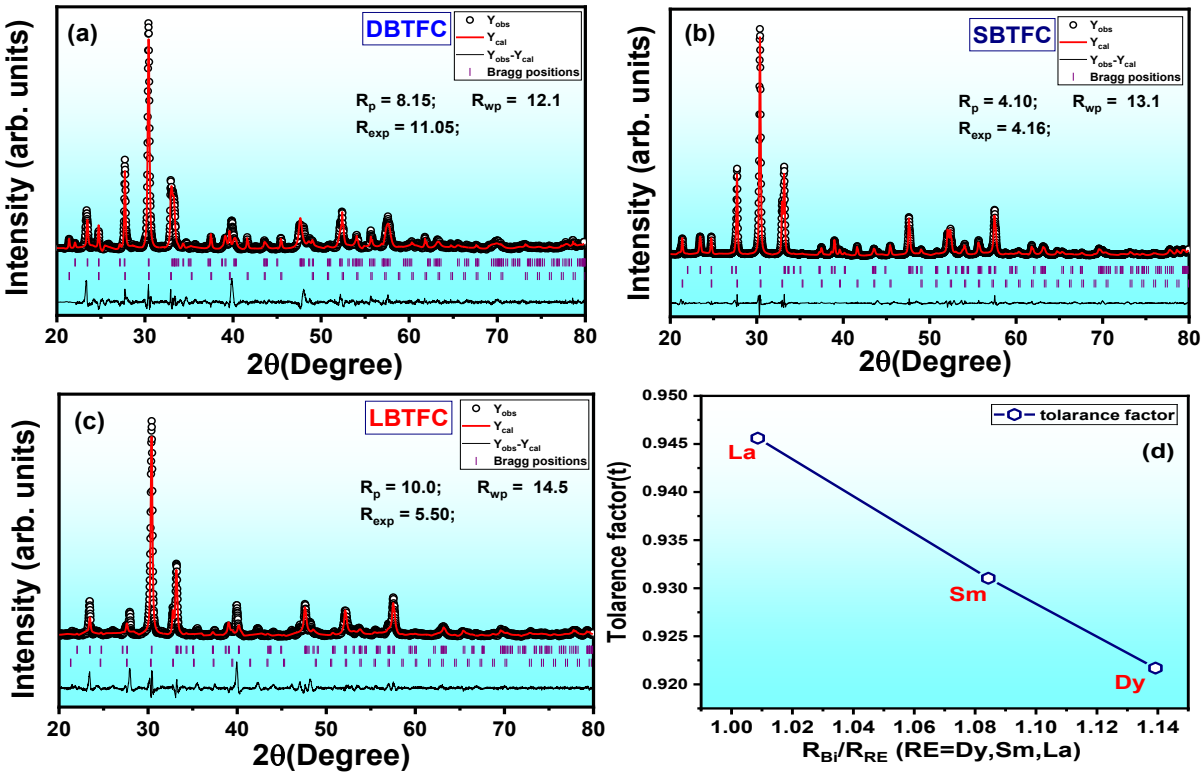

that

Figure 1(a-c) Rietveld refinement of XRD patterns of the BDTFC, BSTFC, and BLTFC ceramics LBTFC (d) tolerance factor τ vs R_{Bi}/R_{RE}

all compounds possess a single phase with an orthorhombic structure with a $Bi_{12}Fe_{0.5}Ti_{0.5}O_{20}$-like impurity phase of space group I23. From the XRD studies, one can conclude that the pyrochlore formation is mainly due to the substitution of heterovalent elements (Ti^{4+}, Fe^{3+}, and Co^{2+}) in the B-site of the ABO_3 perovskites of the Aurivillius phase compounds[55,57]. The reliability parameters (R_p, R_{wp}, and R_{exp}) and goodness of fitting (χ^2) are within the specified range and well-matched between theoretical and experimental diffraction patterns. The experimental and theoretical values of reliability (R)-factors reveal the quality of the phase formation of compounds and the observed error was found to be less than 15% for higher present structured phases [58,59]. Here, the Pseudo-Voigt function is adopted to refine the XRD patterns.

Table 1. Structural parameters of (a)DBTFC (b) SBTFC (c) LBTFC

Sample name	DBTFC		SBTFC		LBTFC	
Space group	Fmmm	I23	Fmmm	I23	Fmmm	I23
Lattice parameters (A^0)	a = 5.415 b = 5.381 c = 32.231	a = 10.173	a = 5.401 b = 5.400 c = 32.331	a = 10.175	a = 5.401 b = 5. 399 c = 32.291	a = 10.220
Volume(A^0)^3	939.348	1052.865	943.087	1053.57	941.709	1067.462
Volume fraction (%)	82.300	17.700	79.78	20.22	99.70	0.300
Space group	Fmmm	I23	Fmmm	I23	Fmmm	I23

Table 2. Structural parameters of (a)DBTFC (b) SBTFC (c) LBTFC

Sample name	DBTFC	SBTFC	LBTFC
Orthorhombic Distortion (b/a)	0.993	0.9998	0.9996
Tetragonal strain (c/a)	5.9521	5.9861	5.9787
Orthorhombicity (2(a-b)/(a+b)*10^2)	0.629	0.018	0.003

The tolerance factor (τ) explains the perovskite nature of the samples. It is reported that τ<1 indicates perovskite nature. From these values, one can understand the tilt of TiO_6 octahedra, which is mainly responsible for dielectric relaxations in the layered perovskite compounds. The tolerance factor for the present compounds was calculated by using the following equation:

$$\tau = \frac{R_A + R_O}{\sqrt{2}\,(R_B + R_O)} \quad (1)$$

Where the terms R_A, R_B, and R_O represent the ionic radii of A-site, B-site, and Oxygen ions respectively. The variation of tolerance factor with the ratio of R_{Bi}/R_{RE} is shown in Fig.1d. The size of RE ionic radii is smaller than the Bi^{3+}(1.35A°) and follows Hume-Rothery conditions and therefore one can says that RE ions can readily be substituted with Bi^{3+} sites. The changes observed in the tolerance factor are due to the changes observed in A-O and B-O bond lengths, which would reflect in the octahedral tilt. More aspects of this would be seen in the Raman spectra, near 800cm^{-1} of stretching of TiO_6 Raman modes. The lattice parameters (a, b, c) and volumes are given in Table 1. The most intense peak is observed around 30^0 and indexed as (1 1 7). The intensity of the peak associated with the (117) plane of $Bi_4Ti_3O_{12}$ is highest, indicating that the prepared ceramic composition conforms to the three-layered structure (m = 3). The result is consistent with common reporting of the strongest diffraction reflection, corresponding to (*1, 1, 2m+1*) reflection in the Aurivillius phase 3-layered compound [56].

3.2 Morphological studies

The morphological images of the prepared ceramics are carried out by FESEM (Field emission scanning electron microscope) as shown in Fig. 2(a-c). The randomly oriented plate-like grains are observed in all ceramics. This kind of surface morphology is a characteristic nature of Aurivillius phase ceramics [60]. It is also observed that all grains are non-uniform and closely packed. The experimental densities of pellets are measured to be roughly 98%. Based on the mentioned values, the samples were found to be denser. The

histograms of grain sizes are drawn and well-fitted by the Gaussian distribution function as shown in the inset of Fig. 2(a-c). The mean grain sizes of the pellets are observed to be ~ 0.492, 0.490, and 0.496 μm for DBTFC, SBTFC, and LBTFC respectively.

Furthermore, grains associated with impurity phases are found in all samples and circled in the SEM pictures. The presence of an additional magnetic phase in the refining data is obvious. The same can be deduced from the presence of the magnetic (Fe/Co) impurity phase due to either heterovalent element substitution in B-sites of perovskites [61]. EDAX (energy dispersion X-ray spectrum) studies are performed on all samples to calculate the elemental composition, as shown in the inset Table in Fig. 3(a-c). Based on the SEM photographs, one can speculate that the pyrochlore or secondary phase or mixture of Fe^{2+}/Co^{2+} ratio. Similar results were more pronounced in the intergrowth Aurivillius phase compounds [63]. It is also observed that grain size and uniformity are found to the more LBTFC. Moreover, one cannot rule out the appearance of plate-like morphology along with micro-pores indicating the low-density nature (>97%) of the sample. As a result, the element composition in all samples was found to be closer to the expected values, and it can be concluded that Fe^{3+} and Co^{2+} ions were segregated into the grain boundary region.

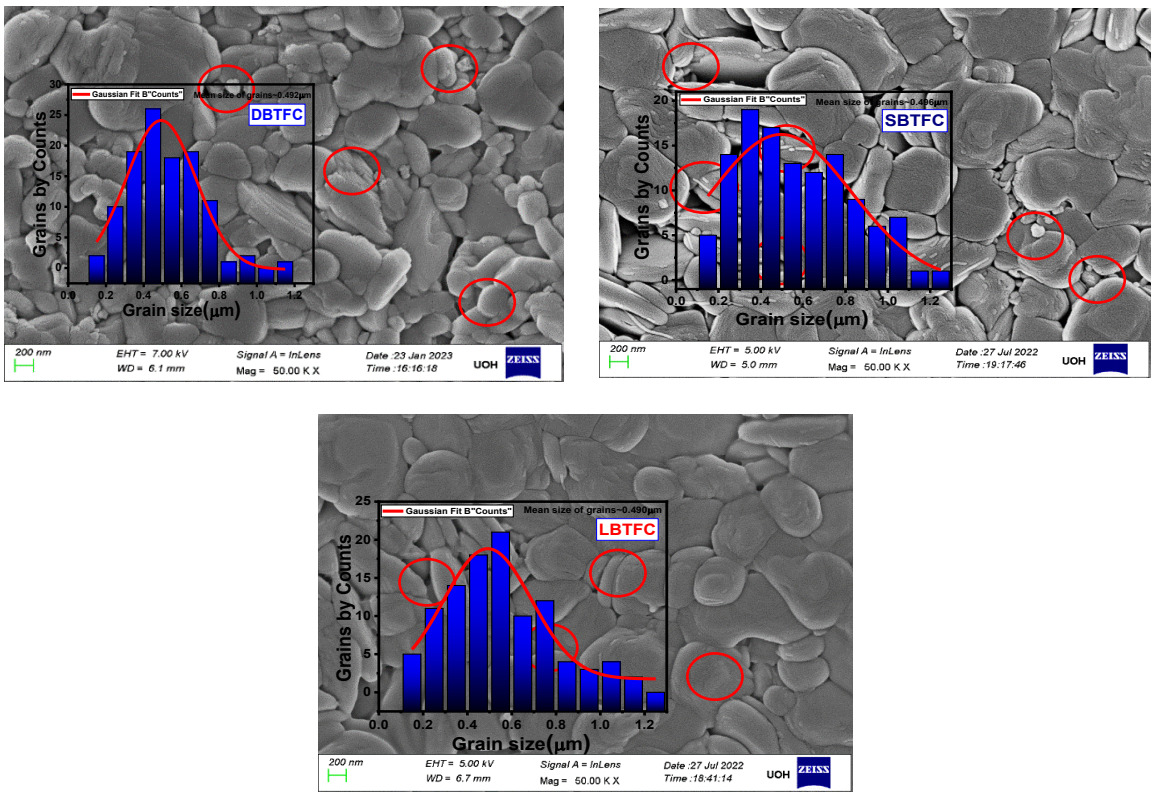

Figure 2(a-c) FESEM photographs of (a)DBTFC (b) SBTFC (c) LBTFC; Inset of Figs. Histograms of the samples

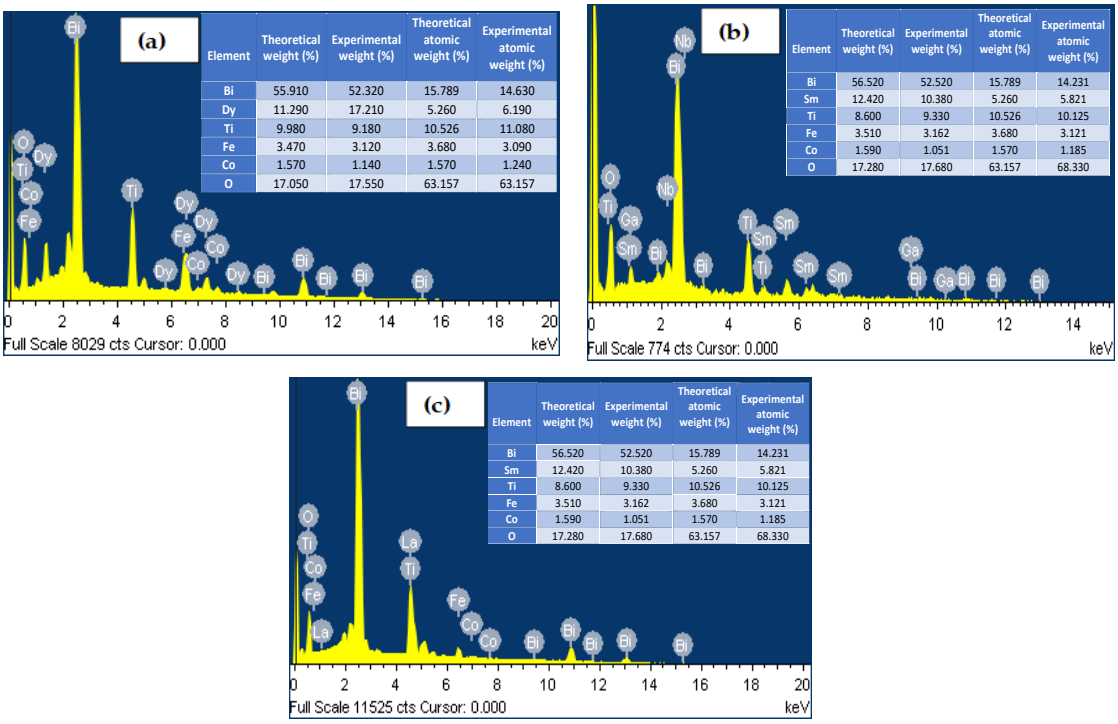

Figure 3(a-c) EDAX patterns of (a) DBTFC (b) SBTFC (c) LBTFC: Inset Figs: Elemental analysis of samples

3.3 Raman spectroscopic studies

Raman scattering spectra of prepared ceramics are shown in Fig. 4(a-c) in order to investigate lattice vibrational modes, lattice distortion, and occupancy of doped ions at the specified A- and B-sites. All observed modes of the prepared samples have shown similar to characteristic modes of the orthorhombic structure of three-layered Aurivillius compounds [57,62,63]. The overlapped peaks were de-convoluted by using Lorentzian

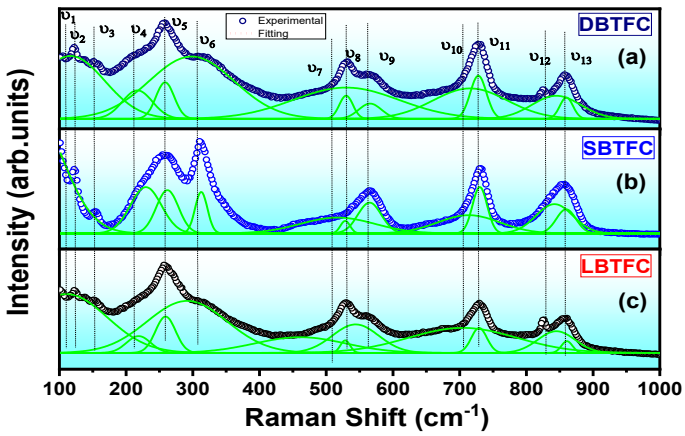

Figure 4(a-c) Raman spectra of (a)DBTFC (b) SBTFC (c) LBTFC

peak fittings, for better identification of peak positions. The Raman modes ν_1, ν_2, and ν_3 below 200 cm^{-1} were attributed to the A- site of ABO_3 perovskite blocks cation vibrations. Slight changes observed for SBTFC, below 200cm^{-1}, is associated with the vibration of Bi^{3+} ions of $(Bi_2O_2)^{2-}$ layer slabs. Changes observed below 200 cm^{-1} for SBTFC, are due to strains caused in the layer-perovskite slabs. The phonon modes at high frequencies in the range of 200 cm^{-1} - 800 cm^{-1} are attributed to the vibrational modes of BO_6 octahedra [64]. The Raman modes ν_4, ν_5, and ν_6 (around 225 cm^{-1}, 260 cm^{-1}, and 312 cm^{-1}) demonstrate the torsional bending of BO_6 octahedra. The phonon modes ν_7, ν_8, and ν_{13} are ascribed to the

stretching of the O-Ti/O-Fe/O-Co bond. The broad peaks namely ν_7, ν_8, and ν_{13} used to reveal the site occupancies of doped ions in the proposed sites. The broadening of the peaks by merging ν_8, and ν_9 for the SBTFC sample is due to the inhomogeneous distribution in the compositions of the A- and B-sites of perovskite blocks. Finally, this in turn leads to lattice distortion. From this one can say, that the RE and Co/Fe ions readily occupies the A- and B- sites of perovskites [65]. The Raman modes ν_4, ν_5, and ν_6 were found to be slightly different for different RE ion substitutions. The same phenomenon is observed in the vibration modes above 200 cm^{-1} for SBTFC. This is once again attributed to the lattice distortion caused by Fe and Co ion doping in Ti-sites of BO_6 octahedral. The phonon modes ν_{10}, and ν_{11}, around 730 cm^{-1} in all samples are attributed to the FeO_6 and CoO_6 octahedral. Based on this, one can say that the Fe and Co ions are partially occupied by the Ti-sites of the perovskite blocks.

3.4 Dielectric studies

The dielectric measurements of all compounds are carried out on the three samples at different frequencies and shown in Fig. 5(a-c) respectively. The variation of dielectric loss (tanδ) with the temperature in the range of RT to 500^{0}C at 10 kHz, 20 kHz, 30 kHz, 50 kHz, and 100kHz frequencies are shown inset of Fig. 5(a-c). The dielectric constant increases with increasing temperature. A notable dielectric dispersion observed with frequency at high temperatures is due to the presence of thermally activated polarization of charge

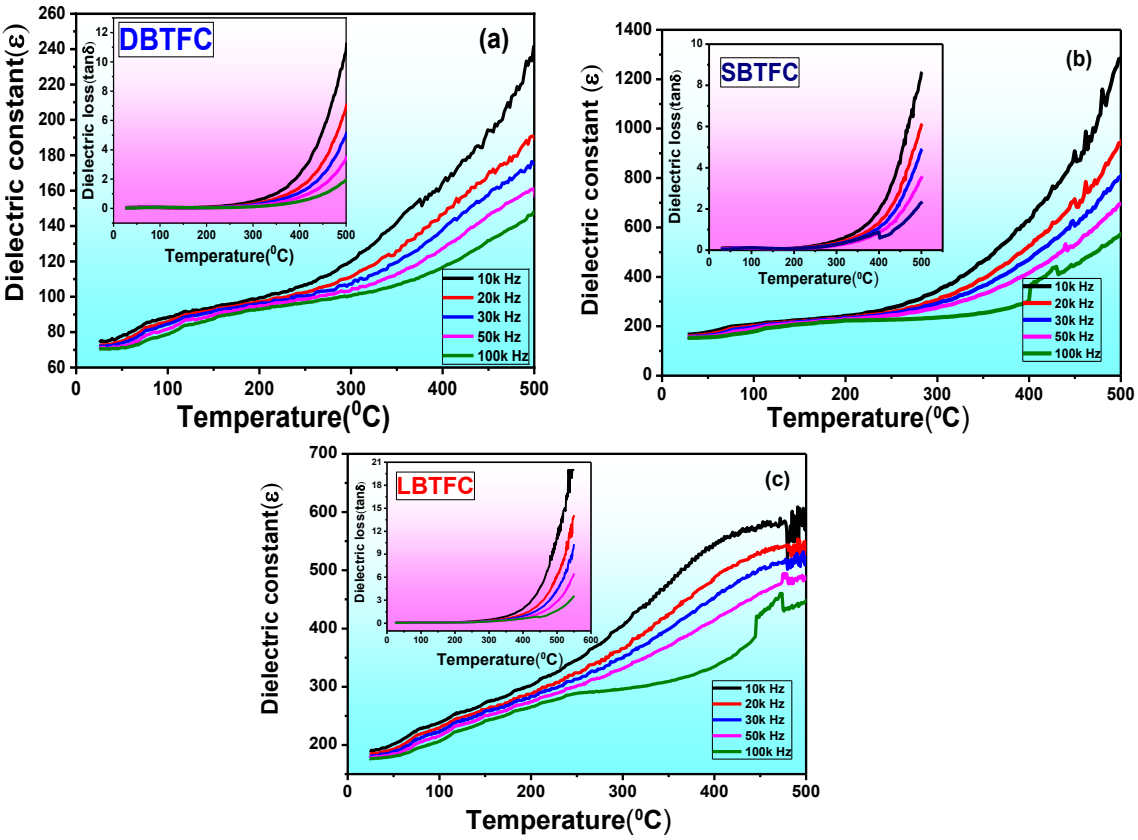

Figure 5(a-c) Variation of dielectric constant with temperature (°C) of (a)DBTFC (b) SBTFC (c) LBTFC; Inset Figs. Dielectric loss vs temperature.

species such as space charges, charge defects, and oxygen vacancies. A slow increase of dielectric nature especially in the DBTFC sample indicates the presence of oxygen vacancies, as pointed out by many researchers. Almost temperature independent of dielectric constant up to 250°C is attributed to hopping conduction mechanism in between the

neighbouring sites of Ti^{3+} and Ti^{4+} or Fe^{2+} and Fe^{3+}. Here forming dipoles with doubly oxygen vacancies (V_O'') is less probable compared to single ionized oxygen vacancies (V_O'). The doubly ionized oxygen vacancies (V''_O) and electrons together create defective or complex dipoles, such as Fe^{3+} – V''_O, Co^{3+}– V''_O, and Ti^{4+}– V''_O. The doubly ionized oxygen vacancies predominate in the conduction process over the singly ionized oxygen vacancies [66]. Generally, the transition temperature of ceramics depends on complex or defective ions. Since the measurements were carried out in the range of RT to 500^0C, the transition temperatures (T_C) of all samples cannot be observed. It is observed that Fe/Co-doped $Bi_4Ti_3O_{12}$ compounds show transition temperatures was found to be more than 600^0C [67–70]. In the present analysis, SBTFC, compounds show a higher dielectric constant than DBTFC, and LBTFC this may be due to an increase in the interfacial or space charge polarization. This increase in the interfacial polarization is observed in the FESEM images. This reveals a decrease in grain size in SBTFC. The decrement in grain size leads to an increase in the interfacial charges due to an increment in the volume fraction of grain boundaries. The same phenomenon is also applicable to the DBTFC and LBTFC samples. A similar conclusion can be inferred from the variation of dielectric loss as a function of temperature, as shown in the inset of Fig. 5(a-c).

3.5 Electrical studies

The AC-conductivity analysis has been performed for a better understanding of the transport mechanism in the samples. Fig. 6(a-c) depicts the AC-conductivity (σ_{ac}) as a function of frequency plots (*f*) at various temperatures. The AC-conductivity data was obtained by considering the following expression

$$\sigma_{ac} = \left[\frac{Z'}{Z'^2+Z''^2}\right]\left(\frac{d}{S}\right) \quad (2)$$

Where σ_{ac} is AC-conductivity, Z' and Z'' are real and imaginary values of impedance. The terms d, and S denote the thickness and area of the sample respectively. The ac conductivity data is found to obey the following Jonscher's power

$$\sigma_{ac} = \sigma_{dc} + A(T)\omega^n \quad (3)$$

Where σ_{ac} is ac conductivity, σ_{dc} is DC-conductivity, A(T) is temperature dependent coefficient, and the exponent n represents slope. The term $A(T)\omega^n$ characterizes the dispersion phenomena observed in the samples. The exponent n is a dimensionless quantity that generally lies between 0 and 1. This quantity depicts the degree of interaction between mobile ions and the surrounding lattice. Attempts were made to fit the ac conductivity data with equation (2), but no data was found to fit successfully throughout the frequency region. From the ac conductivity plots, we can observe two regions namely high-frequency and intermediate-frequency regions as shown in Fig. 6(a-c). The ac conductivity in the low frequency (region-I) is merely independent of frequency. To account for better fitting, the experimental data have been fitted with the following relation

$$\sigma_{ac} = \sigma_{dc} + A(T)\omega^{n_1} + B(T)\omega^{n_2} \quad (4)$$

Where $n_1 (0 < n_1 < 1)$ and n_2 $(1 < n_2 < 2)$ are frequency exponents, which give slopes of corresponding regions. The exponent n_1 depicts the intermediate-frequency dispersion attributing to the ion hopping mechanism. The exponent n_2 describes high-frequency dispersion, attributing to the localized relaxation process [71, 72]. The experimental data is in good agreement with fitting data using equation (4) as shown in Fig. 6(a-c). The ac-conductivity of all samples is more or less strongly independent of frequency above 400^{0}C. The ac-conductivity $\leq 10^4$ Hz is independent of frequency (ω) at all temperatures and provides DC-conductivity. At a temperature below 400^{0}C, the ac-conductivity becomes strongly dependent on frequency for all samples. Strong coalitions or merging into a single curve at higher frequencies for all samples indicates the migration of oxygen vacancies. The exponent values n_1 and n_2 were plotted against temperature Fig. 6(d).

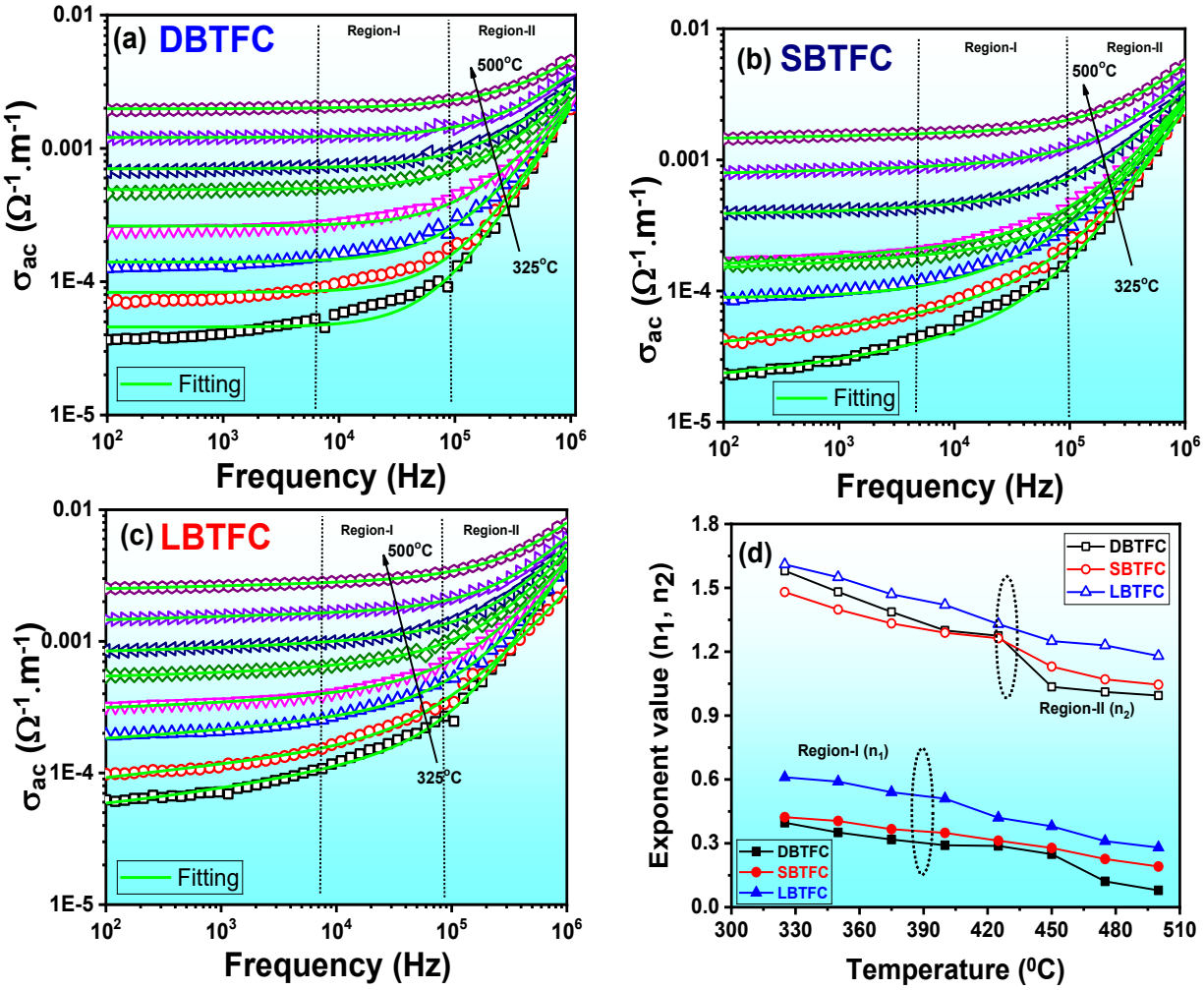

Figure 6(a-c) Variation of AC-conductivity with frequency of (a)DBTFC (b) SBTFC (c) LBTFC; (d) exponent values (n_1, n_2) vs temperature

The frequency-independent conductivity at lower frequencies for all samples can be illustrated by using the ion-jump relaxation model [73,74]. The defective ions that are oxygen vacancies, hop between their neighbourhood vacant sites of Ti^{3+} and Ti^{4+}. This hoping of ions may take a long time and results in a long-range transitional motion of ions. This process is known as the DC-conductivity of the samples. The correlated barrier hopping model can generally explain the frequency-dependent conductivity. From the fitting data, the frequency exponent n_1 decreases with increasing temperature as shown in Fig 6(d). A cation in the lattice is hopping either a forward or backward vacant site. And thermally

active oxygen vacancies yield to more dispersive nature at lower frequencies [75]. Frequency exponent n illustrates the motion or localization of charge carriers in the samples. In region-I (R1), where $0 < n_1 < 1$, the charge carriers can have translation motion and a sudden hop takes place, whereas for $1 < n_2 < 2$ illustrates a localized relaxation or hopping mechanism in the vicinity of lattice sites. Here exponent n_1 values are less the 1, hence the charge carriers have translational ion hopping within the ceramics [71, 76, 77]. On the other side, the values of n_2 are greater than 1 at a higher frequency range, which illustrates the existence of a localized relaxation process. From this analysis, one can speculate that the conductivity is mainly due to short-range hopping or a kind of competitive interaction via doubly ionized oxygen vacancies.

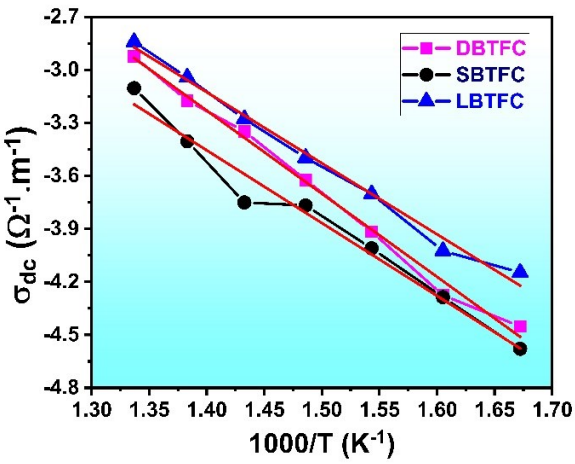

Figure 7 Variation of DC-conductivity with 1000/Temperature (°C) of (a) DBTFC (b) SBTFC (c) LBTFC.

The DC-conductivity of the samples is calculated from AC-conductivity plots by extrapolating the frequency-independent term to 1Hz. Fig. 7 shows DC-conductivity as a function of temperature. The increase in conductivity with increasing temperature indicates the negative temperature coefficient of resistance behaviour. The variation of DC-conductivity with temperature can explain the overall conduction (bulk) of the samples. The activation energies were calculated by using the following Arrhenius relation

$$\sigma_{dc} = \sigma_0 e^{-E_a/KT} \tag{5}$$

Where σ_{dc} is DC-conductivity, E_a is activation energy, T is temperature and K is Boltzmann constant. The variation of DC-conductivity plots reveals the conduction of a thermally activated rotation of dipoles. From the plots, activation energies are observed to be 0.931, 0.828, and 0.807 eV for DBTFC, SBTFC, and LBTFC respectively. From the previous reports, the activation energies of Aurivillius compounds are observed to lie in the order of 0.87eV-1.4eV. The present activation energy values are in good agreement with previous reports [78]. Aurivillius phase compounds have the volatile nature of bismuth during high sintering temperatures. To conserve charge neutrality, certain oxygen loss occurs, as per the following Kroger-Vink notations:

$$\begin{aligned} Bi_2O_3 &\rightarrow 2Bi + 3/2\, O_2 + 2V''_{Bi} + 3V_O \\ V_O &\rightarrow V'_O + e' \\ V'_O &\rightarrow V''_O + e' \end{aligned} \tag{6}$$

Where, V_{Bi}'' is doubly ionized bismuth vacancy, e' is electron released V_O' and V_O'' are singly and doubly ionized oxygen vacancies respectively. The overall conductivity can be attributed to oxygen vacancies and ion valance fluctuations. The ion valance fluctuations in the present samples can be explained as follows:

$$Fe^{3+} + e' \leftrightarrow Fe^{2+}$$

$$Co^{3+} + e' \leftrightarrow Co^{2+} \quad (7)$$

$$Ti^{4+} + \quad e' \leftrightarrow Ti^{3+}$$

From the above equations, Fe^{2+} and Ti^{4+} sites form dipoles with vacant defect (oxygen vacancy). These dipoles try to orient themselves by means of electron electron-hopping mechanism. The charge carriers get trapped near localized sites and may form large polaron. The same phenomenon can apply to the Fe^{2+} ions, where the conduction mechanism is attributed to small polaron.

A more aspect of the above defect mechanism can be corroborated by the complex impedance (Cole-Cole) plots, as shown in Fig. 8 (a-c). The first big and second small semicircles represent the grain (g) and grain boundary (gb) contribution of the samples. large grain resistance (Rg) indicates that the defect such as oxygen vacancies and complex dipoles at grain interfaces, this interim affects the single domain or ferroelectric nature of the samples, more or less grain and grain boundary contributions were observed in the case of $Bi_{3.25}La_{0.75}Ti_3O_{12}$ (BLT) compound [46]. All fitting parameters were depicted in Table 3(a-c). Inset Fig. 8(a-c) exhibits the room temperature hysteresis (Polarization vs Electric field) loops of the DBTFC, SBTFC, and LBTFC samples under the applied strengths of 500V/cm, 750V/cm, and 1000V/cm with a constant frequency of 50 Hz. The unsaturated loops reveal very high coercive and saturation fields. Generally, the Aurivillius phase compounds show low remanent polarization and high coercive and saturation fields. In addition, the polarization of Aurivillius phase compounds is complex and depends on factors such as crystal symmetry, strain effects, phase transitions, and the competency of dopants. The substitution of RE ions in the sites of Bi^{3+} of perovskites of Aurivillius phase compounds causes lattice distortion in the BO_6 octahedron, which affects the electric dipole moments [57]. The asymmetric and unsaturated PE loops illustrate the leaky nature or account of the presence of a greater number of oxygen vacancies or defective charge carriers. It is a known fact that ferroelectric (hysteresis) nature is considered as a collective nature rather than a single ionic migration. Since the overall conductivity is ascribed to the migration of oxygen vacancies or complex defect dipoles at lower temperatures, therefore one cannot get saturated hysteresis loops. This result is an enhancement of the magnetic nature of the samples. From this $Bi_{3.25}La_{0.75}Ti_3O_{12}$ impedance data observation, it is evident that complex-defect

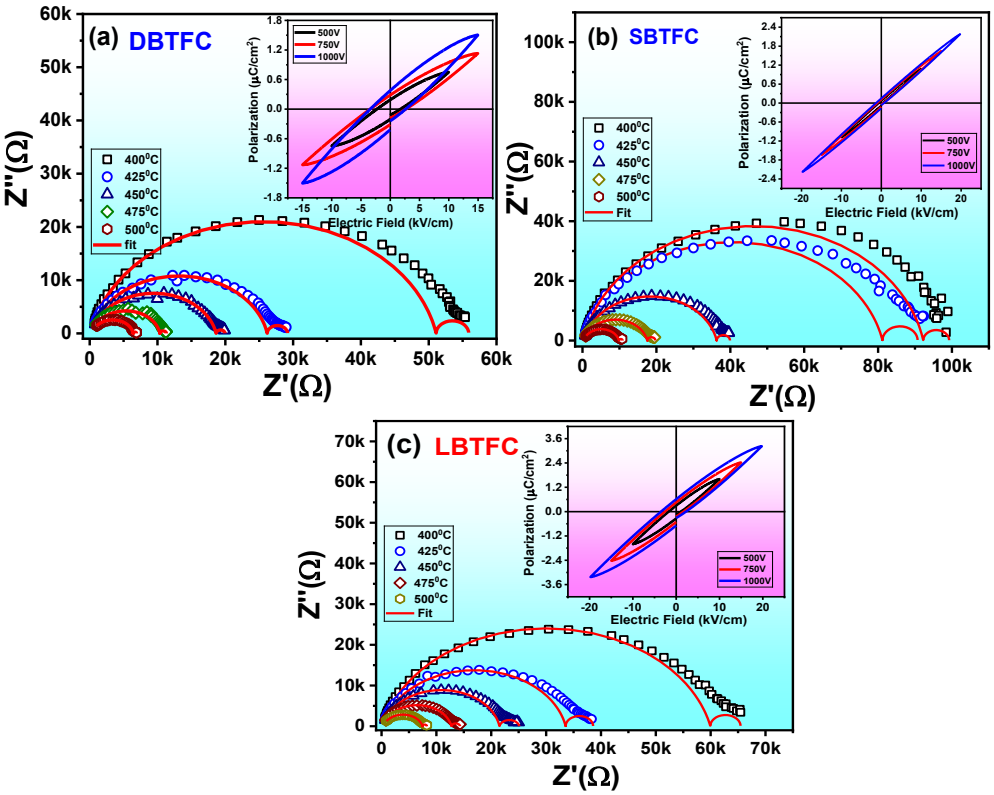

Figure 8(a-c) Complex impedance (Cole–Cole) plots of (a)DBTFC (b) SBTFC (c) LBTFC; Inset Figs. Dielectric loss vs temperature: Inset of Figs P vs E loops.

Table 3(a). Complex impedance fitting parameters DBTFC sample

No.	Temperature	$R_1(\Omega)$	$R_2(\Omega)$	CPE-1	n	$R_3(\Omega)$	CPE-2	n
1	400	200	92000	5.200E-10	0.885	7000	3.40E-4	1
2	425	240	84000	7.500E-10	0.87	6500	4.20E-4	1
3	450	320	36000	6.200E-10	0.875	3600	4.60E-4	1
4	475	340	17200	4.9E-10	0.88	2200	4.65E-4	1
5	500	360	9500	7.80E-10	0.86	1050	5.20E-4	1

Table 3(b). Complex impedance fitting parameters SBTFC sample

No.	Temperature	$R_1(\Omega)$	$R_2(\Omega)$	CPE-1	n	$R_3(\Omega)$	CPE-2	n
1	400	100	51000	6.100E-10	0.877	4800	9.9E-4	1
2	425	180	26000	5.700E-10	0.882	3000	9.1E-4	1
3	450	250	18400	5.500E-10	0.885	1300	8.2E-4	1
4	475	350	10100	4.400E-10	0.895	950	7.9E-4	1
5	500	380	6041	5.300E-10	0.90	480	7.8E-4	1

Table 3(c). Complex impedance fitting parameters LBTFC sample

No.	Temperature	$R_1(\Omega)$	$R_2(\Omega)$	CPE-1	n	$R_3(\Omega)$	CPE-2	n
1	400	150	59800	9.900E-10	0.862	6000	5.0E-4	1
2	425	280	33284	6.400E-10	0.880	5000	4.1E-4	1
3	450	300	21200	6.200E-10	0.89	3600	4.5E-4	1
4	475	320	12400	6.1E-10	0.886	1600	4.7E-4	1
5	500	350	7100	9.50E-10	0.86	800	5.2E-4	1

dipoles which were accumulated at the grain interfaces get relaxed easily during the conduction mechanism, therefore similar compound $Sm_{0.75}Bi_{3.25}Ti_{2.9625}V_{0.03}O_{12}$ (SBVT), rare-earth doped Aurivillius multiferroics had shown well-saturated P-E loops [59, 79]. It suggests that when Ti^{4+} ions were replaced by Fe^{3+} or Co^{3+}. These defective charge complexes were trapped by the oxygen vacancies and hence, higher electric fields are required to activate these trapped charges to get saturated P-E hysteresis loops. Within the applied electric fields, all samples show a less loss nature

3.6 Magnetic studies

The Fig. 9(a-c) shows the variation of magnetization with the applied magnetic field (M-H loops) for all DBTFC, SBTFC, and LBTFC samples obtained at room temperature. Small hysteresis loops with less hysteresis area indicate canted antiferromagnetic (AFM) nature. This nature correlates to the tilt-canted magnetic dipole moments. It should be noted that pure antiferromagnetic samples do not exhibit any hysteresis loop and the canted nature of two sub-lattices yields to small hysteresis loop area. These materials consist of spontaneous magnetized domains. These materials possess low retentively and coercivity values even at high magnetic fields. The introduction of magnetic ions Ni/Fe/Co in the B-site of Aurivillius phases gives raises the spontaneous magnetization [80]. The magnetization in the Co/Fe doped Aurivillius phase compounds main contributions viz (i) exchange interactions between the neighbouring ions like Fe^{3+}– O – Co^{2+} or Fe^{3+}– O – Co^{3+} in iron-rich regions. (ii) tilt–canted spins or antisymmetric DM (Dzyaloshinskii-Moriya) interactions. In three layered single-phase Aurivillius compounds with orthorhombic Fmmm structure, exhibit AFM or weak ferromagnetism, which is emerged from the localized magnetic (Fe/Co) rich regions. This suggests the super-exchange interaction between neighbouring Fe and Co ions via oxygen vacancies [81,82]. This can also be due to the long-range magnetic order in the ceramics. Another possible explanation is on account of magnetization the structural distortion of the perovskite slabs. The structure evolution and Fe/Co – O – Co/Fe bond angles in ABO_3 perovskites in the layered compounds also affect the magnetization of the ceramics.

$$M = M_S \left[1 - \frac{A}{H} - \frac{B}{H^2}\right] + \chi_P H_K \quad (8)$$

The represent $\frac{A}{H}$ represents the inhomogeneity of magnetic nature, and $\chi_P H_K$ is the forced field induced magnetization, and $\frac{B}{H^2}$ parameters explain magneto-anisotropic nature. By considering the importance of the above LAS, equation 8 is fitted in the low magnetic field regions and shown in the inset of Fig. 9(a-c). By using equation 8, the output of fitting curves (R^2) was found to be ~0.99 and thus the results of fitting were highly reliable.

In the present investigation, sample DBTFC shows an unsaturated hysteresis nature,

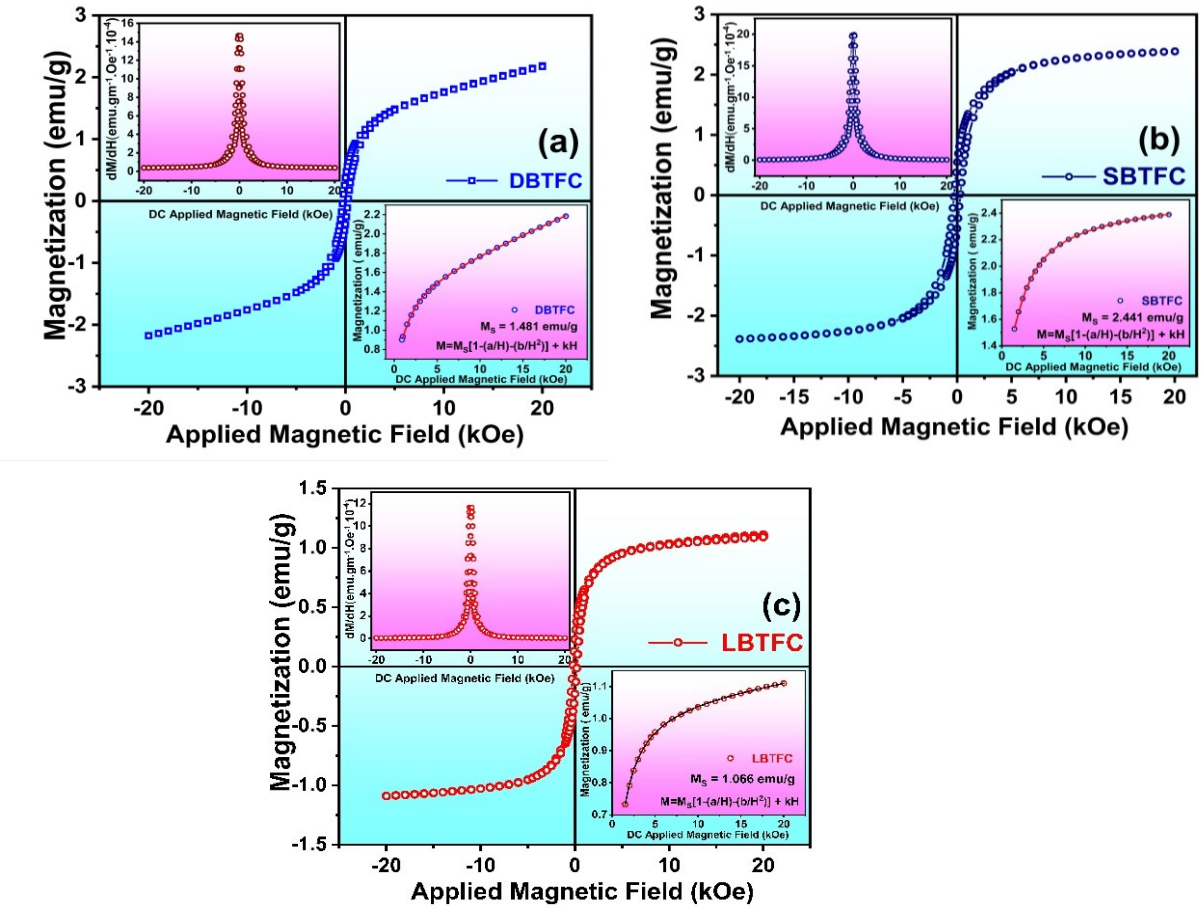

Figure 9(a-c) Com Variation of Magnetization vs Applied Magnetic of (a)DBTFC (b) SBTFC (c) LBTFC; Inset Figs. (left) derivation of magnetization (dM/dH) vs applied magnetic field; Inset Figs (Right) Law of approach to saturation fittings M vs. H curves of DTFCS, SBTFC, and LBTFC samples.

indicating the combination of both FM and AFM [83]. The formation of Bi – O – Dy bonds enhances the magnetization, thereby the Dy^{3+} and Fe^{3+}/Co^{3+} ions contribute to the magnetization. The Sm^{3+} doped REBTFC sample shows a higher value of magnetization. The results are consistent with our previous work [57]. The SBTFC sample exhibits remanent magnetization (2Mr) of about 550 memu/g at room temperature, which is bigger than the earlier reported value[84,85]. The inset of Fig. 9(a-c) (left) illustrates the plots of the derivation of magnetization (dM/dH) as a function of the applied magnetic field. It can be noticed that a single sharp peak is observed in all curves. This can be attributed to the behaviour of soft kind magnetism and uniform magnetic grain nature. A single sharp peak is observed in the left side inset of Fig. 9(a-c). From this one can anticipate that all prepared samples are of a soft kind of magnetic nature

3.7 Magnetoelectric studies

The variation of the magnetoelectric (ME) coefficient with the applied magnetic field of prepared samples is shown in Fig.10. The values of the magnetoelectric coefficient have been found 42.4 mV/cm-Oe, 30.3 mV/cm-Oe, and 21.6 mV/cm-Oe for DBTFC, LBTFC, and SBTFC respectively.

It is observed from the previous reports that the $Bi_4Ti_3Fe_{0.7}Co_{0.3}O_{15}$ (BFTO) sample has shown an ME coefficient of 16.45 mV $cm^{-1}Oe^{-1}$[64, 86]. The obtained ME values of the prepared samples are found to be higher compared to the other Aurivillius compounds. Furthermore, the high ME coefficient is obtained at lower magnetic fields (3kOe) as shown in Fig. 10. The ME coupling mainly arises from two aspects, namely, (i) spin-exchange or

spin-orbit interactions, driven by inverse DM interaction, and (ii) spin-lattice interaction. The contribution of spin-orbit or spin-exchange interaction via inverse DM interactions is comparatively smaller than the spin-lattice interactions [87]. In particular, the magnetic ions in BO_6 octahedral sites are slightly shifted from their regular sites under the application of a magnetic field. This induces a strain in the lattice structure and develops the voltage via ferroelectric accumulated changes. However further studies are needed to establish the plausible reason for getting a high ME coefficient. As it is reported that, the impurity phases of Co/Fe compositions influence the ME nature in Aurivillius compounds [57]. The presence of circled regions of SEM micrograph dots (nanoregions), represent Co/Fe-rich magnetic phase. Based on these observations, such Co/Fe-rich phases could contribute partly to the enhanced ME properties of the prepared samples.

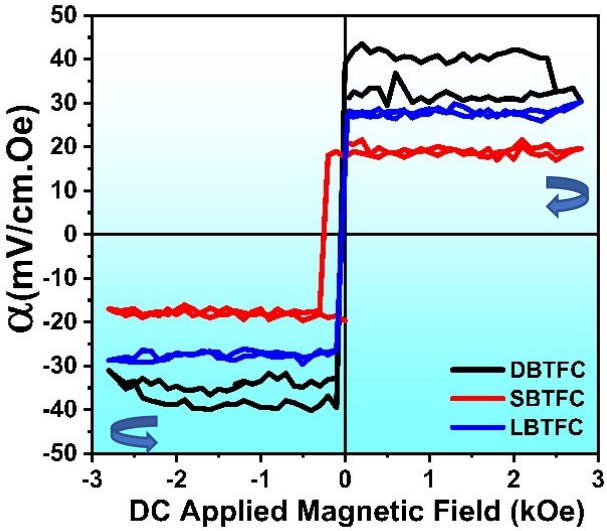

Figure10. Magnetoelectric coefficient vs applied magnetic field plots of (a) DBTFC (b) SBTFC (c) LBTFC samples.

In particular, when an external magnetic field is applied, the magnetic ions are slightly displaced from their normal octahedral position, which induces a voltage in the lattice, resulting in ferroelectric and ferro-elastic changes, and finally producing an output voltage. The parameters orthorhombic distortion, tetragonal stain, and Orthorhombicity play a significant role in ME properties [88]. In our study, the DBTFC sample as shown higher ME coefficients. This is in good agreement with the lattice structure of the prepared samples Higher Orthorhombicity and lower orthorhombic distortion values are observed for Dy doped sample (DBTFC), which are favourable to enhancing the ME coefficient under magnetic fields. From this study, the RE (Dy, La, and Sm) element substitution in the A-site of Aurivillius compounds induces lattice distortion, and it leads to accompanying electric polarization under magnetic fields. It can be concluded that the RE-doped three–layered Aurivillius phase compounds show strong ME coupling. These multiferroic materials are useful for understanding the ME phenomenon.

4. Conclusions

In summary, we have investigated the structural, morphological, electrical, magnetic, and magnetoelectric properties of the RE (Dy, Sm, and La) doped $Bi_3RETi_2Fe_{0.7}Co_{0.3}O_{12-\delta}$ Aurivillius multiferroic compounds. The XRD and Raman spectroscopic studies reveal that the prepared samples are formed in single phase and orthorhombic structure with space group *Fmmm*. This reveals that the ions are properly substituted into lattice cells. The plate-like, anisotropic randomly orientated grains are observed in FESEM studies, which is a characteristic feature of Aurivillius phase ceramics. The

substitution of RE enhances significantly the dielectric and ferroelectric properties with improved dielectric constants in frequency range and reduced dielectric loss values are found at lower frequency ranges. The improved remanent polarization is observed in all samples at room temperature. This is attributed to the reduction in the oxygen vacancies by doping RE in the Bi-sites of the samples. The ferroelectric and magnetic studies reveal good multiferroic behaviour in the samples. The M-H loops of the samples suggest the exchange interaction between adjacent ions or DM interactions among magnetic ions. The strong ferroelectric-magnetic coupling accompanied by a high coefficient of magnetoelectric coupling of 42.4 mV/cm-Oe, was exhibited by the DBTFC sample. This strong ME coefficient in a single phase may be applicable in multiferroic devices can be interpreted from the perspective of previous studies and of the working hypotheses.

Author Contributions: Conceptualization V.V., N.V.P. E.V.R; Methodology: V.V Data curation, V.V, VSP, S.N.B: Writing – original draft preparation V.V; writing and reviewed work: NVP, EVR, G.S., G.P; Supervision: NVP, GP. All authors have read and agreed to the published version of the manuscript.

Funding: Please add: This work was partially supported by OU-DST PURSUE-II/80//2021 and CSIR-HRDG, No: 09/132(0875)/2018-EMR-I, New Delhi for providing Fellowship.

Data Availability Statement: Not applicable

Acknowledgments: One of the authors (V V) is thankful to CSIR-HRDG, New Delhi for providing JRF/SRF (File No: 09/132(0875)/2018-EMR-I). One of the authors (NVP) acknowledges the funding by AR&DB project 2004, OU-DST PURSUE-II/80/2021, SIR-HRDG and 09/132(0875)/2018-EMR-I, New Delhi. EVR (032-88-ARH/2018) acknowledges the Portuguese foundation for science and technology (FCT) for financial assistance through national funds (OE), in the scope of the framework contract foreseen in the numbers 4, 5, and 6 of article 23of the Decree-Law 57/2016, of August 29, changed by Law 57/2017, of July 19. The research at Oakland University was supported by grants from the National Science Foundation (ECCS-1923732, ECCS-EAGER-2236879) and the Air Force Office of Scientific Research (AFOSR) Award No. FA9550-20-1-0114. "

Conflicts of Interest: The authors declare no conflict of interest.

References

[1] C.W. Nan, M.I. Bichurin, S. Dong, D. Viehland, G. Srinivasan, Multiferroic magnetoelectric composites: Historical perspective, status, and future directions, J. Appl. Phys. 103 (2008).

[2] M. Bibes, A. Barthélémy, Multiferroics: Towards a magnetoelectric memory, Nat Mater 7 (2008) 425–426.

[3] S. Dong, J.M. Liu, S.W. Cheong, Z. Ren, Multiferroic materials and magnetoelectric physics: Symmetry, entanglement, excitation, and topology, Adv. Phys. 64 (2015) 519–626.

[4] M. Fiebig, T. Lottermoser, D. Meier, M. Trassin, The evolution of multiferroics, Nat. Rev. Mater. 1 (2016).

[5] D. Khomskii, Classifying multiferroics: Mechanisms and Effects, Physics (College Park Md) 2 (2009).

[6] N.A. Spaldin, Multiferroics: Past, present, and future, MRS. Bull. 42 (2017) 385–389.

[7] B. Jana, K. Ghosh, K. Rudrapal, P. Gaur, P.K. Shihabudeen, A. Roy Chaudhuri, Recent Progress in Flexible Multiferroics, Front Phys 9 (2022).

[8] J.F. Scott, Data storage: Multiferroic memories, Nat. Mater. 6 (2007) 256–257.

[9] J. Kreisel, M. Kenzelmann, Multiferroics - The challenge of coupling magnetism and ferroelectricity, Europhysics News 40 (2009) 17–20.

[10] R.R. Sahoo, R.N.P. Choudhary, Effect of Ce infusion on the structural, dielectric, optical, transport and polarization behavior of Nd-modified triple-layered Aurivillius phase ceramic $Bi_3NdTi_3O_{12}$, Ceram. Int. 50 (2024) 205–217.

[11] E.C. Subbarao, A family of ferroelectric bismuth compounds, Journal of Physics and Chemistry of Solids 23 (1962) 665–676.

[12] G. Wang, Y. Huang, S. Sun, J. Wang, R. Peng, Y. Lu, X. Tan, Layer Effects on the Magnetic Behaviors of Aurivillius Compounds $Bi_{n+1}Fe_{n-3}Ti_3O_{3n+1}$ (n = 6, 7, 8, 9), Journal of the American Ceramic Society 99 (2016) 1318–1323.

[13] V.A. Khomchenko, G.N. Kakazei, Y.G. Pogorelov, J.P. Araujo, M. V. Bushinsky, D.A. Kiselev, A.L. Kholkin, J.A. Paixão, Effect of Gd substitution on ferroelectric and magnetic properties of $Bi_4Ti_3O_{12}$, Mater Lett 64 (2010) 1066–1068.

[14] D. Hou, H. Fan, Y. Chen, Y. Jia, W. Wang, Effects of lanthanide ions on the structure and electrical properties of Aurivillius Bi_3TiNbO_9 high temperature piezoelectric ceramics, J. Alloys. Compd. 921 (2022).

[15] J. Sun, Y. Han, G. Gao, J. Yang, Y. Zhang, Y. Dai, D. Song, Breakdown field enhancement and energy storage performance in four-layered Aurivillius films, Ceram. Int. 48 (2022) 15780–15784.

[16] Z. Li, V. Koval, A. Mahajan, Z. Gao, C. Vecchini, M. Stewart, M.G. Cain, K. Tao, C. Jia, G. Viola, H. Yan, Room-temperature multiferroic behavior in layer-structured Aurivillius phase ceramics, Pubs.Aip.Org 117 (2020) 52903.

[17] S. Supriya, Effect of doping and enhanced microstructures of bismuth titanates as aurivillius perovskites, Micron 162 (2022) 103344.

[18] T. Kikuchi, A. Watanabe, K. Uchida, A FAMILY OF MIXED-LAYER TYPE BISMUTH COMPOUNDS, Pergamon Press, Inc, 1977.

[19] H. Zhao, K. Cai, Z. Cheng, T. Jia, H. Kimura, Z. Ma, Q. Fu, Z. Huang, T. Matsumoto, T. Tohei, N. Shibata, Y. Ikuhara, A Novel Class of Multiferroic Material, $Bi_4Ti_3O_{12}\cdot nBiFeO_3$ with Localized Magnetic Ordering Evaluated from Their Single Crystals, Adv. Electron. Mater. 3 (2017) 1600254.

[20] V. Veenachary, V.S. Puli, S.N. Babu, G. Prasad, N. V. Prasad, Electrical and magnetic studies on promising Aurivillius intergrowth compound, Journal of Materials Science: Materials in Electronics 33 (2022) 22614–22627.

[21] V. Koval, Y. Shi, I. Skorvanek, G. Viola, R. Bures, K. Saksl, P. Roupcova, M. Zhang, C. Jia, H. Yan, Cobalt-induced structural modulation in multiferroic Aurivillius-phase oxides, J. Mater. Chem. C Mater 8 (2020) 8466–8483..

[22] Y. Yin, F. Liu, X. Mao, W. Wang, Multiferroic properties of $Bi_{5.75}R_{0.25}Fe_{1.4}Ni_{0.6}Ti_3O_{18}$ (R = Eu, Sm, Nd, Bi and La) ceramics, Journal of Rare Earths 40 (2022) 112–117.

[23] R.Z. Hou, X.M. Chen, S.Y. Wu, Substitution of Sm^{3+} and Nd^{3+} for Bi3+ in $SrBi_8Ti_7O_{27}$ Mixed Aurivillius Phase, Japanese Journal of Applied Physics, Part 1: Regular Papers and Short Notes and Review Papers 42 (2003) 5169–5171.

[24] N.A. Lomanova, Aurivillius Phases Bim+ 1Fem− 3Ti3O3m+ 3: Synthesis, Structure, and Properties (a Review), Russian Journal of Inorganic Chemistry 67 (2022) 741–753.

[25] S.K. Patri, R.N.P. Choudhary, B.K. Samantaray, Studies of structural, dielectric, and impedance properties of $Bi_9Fe_5Ti_3O_{27}$ ceramics, J. Electroceram. 20 (2008) 119–126.

[26] Z.G. Yi, Y.X. Li, Y. Wang, Q.R. Yin, Dielectric and ferroelectric properties of intergrowth $Bi_{7-x}La_xTi_4NbO_{21}$ ceramics, Appl. Phys. Lett. 88 (2006).

[27] X. Gao, H. Gu, Y.X. Li, Z.G. Yi, M. Čeh, K. Žagar, Structural evolution of the intergrowth bismuth-layered $Bi_7Ti_4NbO_{21}$, J. Mater. Sci. 46 (2011) 5423–5431.

[28] C. Liu, Z. Chen, R. Peng, Z. Fu, X. Zhai, Y. Lu, The structure and properties of Co substituted $Bi_7Ti_4NbO_{21}$ with intergrowth phases, RSC. Adv. 7 (2017) 50477–50484.

[29] N. V. Giridharan, S. Supriya, Effect of processing on the properties of $Bi_{3.15}Nd_{0.85}Ti_3O_{12}$ thin films, Thin Solid Films 516 (2008) 5244–5247.

[30] D. Coathup, Z. Li, X. Zhu, H. Yan, R. Zhang, H. Ye, Dielectric and ferroelectric properties of BTFCO thin films, J. Electroceram. 43 (2019) 92–95.

[31] Y. Li, Z. Li, X. Wang, H. Li, J. Su, H. Zhang, X. He, Z. Chi, L. Liu, Scaling behavior of dynamic hysteresis in multiferroic $Bi_5FeTi_3O_{15}$ thin films, Journal of Materials Science: Materials in Electronics 32 (2021) 27333–27338.

[32] W. Prellier, M.P. Singh, P. Murugavel, The single-phase multiferroic oxides: From bulk to thin film, Journal of Physics Condensed Matter 17 (2005).

[33] F. Huang, X. Lu, T. Xu, Y. Liu, W. Su, Y. Jin, Y. Kan, J. Zhu, Multiferroic properties of Co and Nd co-substituted $Bi_5Ti_3FeO_{15}$ thin films, Thin Solid Films 520 (2012) 6489–6492.

[34] S. Ma, W. Li, J. Hao, S. Ren, M. Wang, Z. Xu, Microstructure and ferroelectric properties of Ta-doped $Bi_{3.25}La_{0.75}Ti_3O_{12}$/ZnO thin film capacitors, Ceram. Int. 48 (2022) 5239–5245.

[35] D. Song, J. Yang, B. Yang, L. Chen, F. Wang, X. Zhu, Evolution of structure and ferroelectricity in Aurivillius $Bi_4Bi_{n-3}Fe_{n-3}Ti_3O3_{n+3}$ thin films, J. Mater. Chem. C Mater. 6 (2018) 8618–8627.

[36] H. Sun, X. Lu, T. Xu, J. Su, Y. Jin, C. Ju, F. Huang, J. Zhu, Study of multiferroic properties in $Bi_5Fe_{0.5}Co_{0.5}Ti_3O_{15}$ thin films, J. Appl. Phys. 111 (2012).

[37] X.Q. Chen, F.J. Yang, W.Q. Cao, H. Wang, C.P. Yang, D.Y. Wang, K. Chen, Enhanced multiferroic characteristics in Fe-doped $Bi_4Ti_3O_{12}$ ceramics, Solid State Commun. 150 (2010) 1221–1224.

[38] X.Q. Chen, Y. Qiao, X.L. Liu, C.J. Lu, G. Le Rhun, S. Senz, D. Hesse, Microstructure and electric properties of (104)/(014)-oriented $Bi_{3.15}Nd_{0.85}Ti_3O_{12}$ films on Pt (111)/Ti/SiO2/Si by sol-gel method, Mater. Lett. 61 (2007) 4897–4900.

[39] N. Sharma, B.J. Kennedy, M.M. Elcombe, Y. Liu, C.D. Ling, Coexistence of ferroelectricity and magnetism in transition-metal-doped n = 3 Aurivillius phases, Journal of Physics Condensed Matter 20 (2008).

[40] J. Halpin, L. Keeney, Naturally Layered Aurivillius Phases: Flexible Scaffolds for the Design of Multiferroic Materials, OAJ Materials and Devices 5 (2021)..

[41] P.C. Joshi, S.B. Desu, Structural and electrical characteristics of rapid thermally processed ferroelectric $Bi_4Ti_3O_{12}$ thin films prepared by metalorganic solution deposition technique, J. Appl. Phys. 80 (1996) 2349–2357.

[42] X. Li, L. Zhu, P. Huang, Z. Chen, W. Bai, L. Li, F. Wen, P. Zheng, W. Wu, L. Zheng, Y. Zhang, Reduction of oxygen vacancy concentration and large enhancement of electrical performances in Cu/Sb co-doped $Bi_4Ti_3O_{12}$ high-temperature piezoelectric ceramics, J. Appl. Phys. 127 (2020).

[43] R. Bokolia, O.P. Thakur, V.K. Rai, S.K. Sharma, K. Sreenivas, Electrical properties and light upconversion effects in $Bi_{3.79}Er_{0.03}Yb_{0.18}Ti_{3-x}W_xO_{12}$ ferroelectric ceramics, Ceram. Int. 42 (2016) 5718–5730.

[44] B.D. Stojanović, C.O. Paiva-Santos, M. Cilense, Č. Jovalekić, Z.Ž. Lazarević, Structure study of $Bi_4Ti_3O_{12}$ produced via mechanochemically assisted synthesis, Mater. Res. Bull. 43 (2008) 1743–1753.

[45] N. V. Prasad, G. Prasad, G.S. Kumar, S. Karmakar, S.M. Gupta, Electrical relaxation studies on lanthanum and vanadium modified $Bi_4Ti_3O_{12}$, Ferroelectrics 437 (2012) 88–102.

[46] C. Lavado, M.G. Stachiotti, Fe^{3+}/Nb^{5+} co-doping effects on the properties of Aurivillius $Bi_4Ti_3O_{12}$ ceramics, J Alloys Compd 731 (2018) 914–919.

[47] W. Wang, X. Shen, W. Wang, X. Guan, Y. Yao, Y. Wang, R. Yu, The Evolution of Microstructure and Magnetic Properties of the Bismuth Layer Compounds with Cobalt Ions Substitution, Inorg. Chem. 56 (2017) 3207–3213.

[48] W.C. Ferreira, G.L.C. Rodrigues, B.S. Araújo, F.A.A. de Aguiar, A.N.A. de Abreu Silva, P.B.A. Fechine, C.W. de Araujo Paschoal, A.P. Ayala, Pressure-induced structural phase transitions in the multiferroic four-layer Aurivillius ceramic $Bi_5FeTi_3O_{15}$, Ceram. Int. 46 (2020) 18056–18062.

[49] S. Shigyo, T. T, T. T., K. Kiyono, H. H., N. Nakano, J. J., I. Itoh, T. Takahashi, Synthesis and dielectric-magnetic properties of rare-earth (La, Nd, Sm)-modified $Bi_4Ti_3O_{12}$, Jpn J. Appl. Phys. 47 (2008) 7617–7622.

[50] J. Paul, S. Bhardwaj, K.K. Sharma, R.K. Kotnala, R. Kumar, Room-temperature multiferroic properties and magnetoelectric coupling in $Bi_{4-x}Sm_xTi_{3-x}Co_xO_{12-\delta}$ ceramics, J Mater. Sci. 49 (2014) 6056–6066.

[51] Z. Yu, X. Meng, Z. Zheng, Y. Lu, H. Chen, C. Huang, H. Sun, K. Liang, Z. Ma, Y. Qi, T. Zhang, Room temperature multiferroic properties of rare-earth-substituted Aurivillius phase $Bi_5Ti_3Fe_{0.7}Co_{0.3}O_{15}$ ceramics, Mater. Res. Bull. 115 (2019) 235–241.

[52] A. Chakrabarti, J. Bera, Effect of La-substitution on the structure and dielectric properties of BaBi4Ti4O15 ceramics, Journal of Alloys and Compounds, 505, 2, 2010, 668-674.

[53] T. Patri, J. Praveen Kumar, A. Ghosh, P.D. Babu, Tunable polarization with enhanced multiferroic response of W/Co co-doped $Bi_4LaFeTi_3O_{15}$ Aurivillius ceramics, J. Appl. Phys. 128 (2020).

[54] M. Algueró, M. Pérez-Cerdán, R.P. del Real, J. Ricote, A. Castro, Novel Aurivillius $Bi_4Ti_{3-2x}Nb_xFe_xO_{12}$ phases with increasing magnetic-cation fraction until percolation: a novel approach for room temperature multiferroism, J. Mater. Chem. C Mater. 8 (2020) 12457–12469.

[55] T.K. Mandal, T. Sivakumar, S. Augustine, J. Gopalakrishnan, Heterovalent cation-substituted Aurivillius phases, $Bi_2SrNaNb_2TaO_{12}$ and $Bi_2Sr_2Nb_{3-x}M_xO_{12}$ (M = Zr, Hf, Fe, Zn), Materials Science and Engineering: B 121 (2005) 112–119.

[56] W.J. Yu, Y.I. Kim, D.H. Ha, J.H. Lee, Y.K. Park, S. Seong, N.H. Hur, A new manganese oxide with the Aurivillius structure: $Bi_2Sr_2Nb_2MnO_{12-\delta}$, Solid State Commun. 111 (1999) 705–709.

[57] V. Veenachary, E.V. Ramana, S.N. Babu, V.S. Puli, A. Srinivas, G. Srinivasan, S. Saha, G. Prasad, N.V. Prasad, Magnetic and Magnetoelectric Properties of AurivilliusThree- and Four-Layered Intergrowth Ceramics, Crystals 2023, Vol. 13, Page 426 13 (2023) 426.

[58] Venkataraman, B.H., Varma, K.B.R. Microstructural, dielectric, impedance and electric modulus studies on vanadium—doped and pure strontium bismuth niobate ($SrBi_2Nb_2O_9$) ceramics. J Mater. Sci: Mater. Electron. **16**, 335–344 (2005).

[59] E.V. Ramana, N. V. Prasad, D.M. Tobaldi, J. Zavašnik, M.K. Singh, M.J. Hortigüela, M.P. Seabra, G. Prasad, M.A. Valente, Effect of samarium and vanadium co-doping on structure, ferroelectric and photocatalytic properties of bismuth titanate, RSC. Adv. 7 (2017) 9680–9692.

[60] Vadla Veenachary, Eskilla Venkata Ramana, Gobburu Subramanya Kumar, Guduru Prasad & Nandiraju Venkata Prasad (2020) Electrical Studies on $Bi_4NdTi_3Fe_{0.7}Co_{0.3}O_{15}$-$Bi_3NdTi_2Fe_{0.7}Co_{0.3}O_{12-\delta}$ Intergrowth Aurivillius Ceramics, Transactions of the Indian Ceramic Society, 79:3, 113-119.

[61] D.L. Zhang, W.C. Huang, Z.W. Chen, W.B. Zhao, L. Feng, M. Li, Y.W. Yin, S.N. Dong, X.G. Li, Structure evolution and multiferroic properties in cobalt doped $Bi_4NdTi_3Fe_{1-x}Co_xO_{15}$-$Bi_3$ $NdTi_2Fe_{1-x}Co_xO_{12-\delta}$ Intergrowth Aurivillius Compounds, Sci. Rep. 7 (2017).

[62] S.R. Das, P.S. Dobal, B. Sundarakannan, R.R. Das, R.S. Katiyar, Micro-Raman study of Zr-substituted $Bi_4Ti_3O_{12}$ ceramics, Journal of Raman Spectroscopy 38 (2007) 1077–1081.

[63] D. Wu, Y. Deng, C.L. Mak, K.H. Wong, A.D. Li, M.S. Zhang, N.B. Ming, Raman scattering study of La-, Nd- And Sm-substituted $Bi_4Ti_3O_{12}$, Appl. Phys. A Mater . Sci. Process. 80 (2005) 607–610.

[64] R. Ti, X. Lu, J. He, F. Huang, H. Wu, F. Mei, M. Zhou, Y. Li, T. Xu, J. Zhu, Multiferroic properties and magnetoelectric coupling in Fe/Co co-doped $Bi_{3.25}La_{0.75}Ti_3O_{12}$ ceramics, J. Mater. Chem. C Mater. 3 (2015) 11868–11873.

[65] J. Paul, S. Bhardwaj, K.K. Sharma, R.K. Kotnala, R. Kumar, Room-temperature multiferroic properties and magnetoelectric coupling in Bi4-x Sm x Ti3-x Co x O 12-δ ceramics, J. Mater. Sci. 49 (2014) 6056–6066.

[66] Z. Yin, Y. Sheng, G. Ma, Dielectric, multiferroic and magnetodielectric properties of Co/Fe co-doped $Bi_4Ti_3O_{12}$ ceramics, Journal of Materials Science: Materials in Electronics 30 (2019) 10483–10490.

[67] C. Long, W. Ren, Y. Li, L. Liu, Y. Xia, H. Fan, High oxide ion conductivity in layer-structured $Bi_4Ti_3O_{12}$-based ferroelectric ceramics, J. Mater. Chem. C Mater. 7 (2019) 8825–8835.

[68] J.P. Kumar, K.S.K.R.C. Sekhar, T.D. Rao, P.D. Babu, P. Tirupathi, Effect of sintering temperature on structural, dielectric, and electrical property studies of $Bi_4NdTi_3FeO_{15}$ aurivillius ceramics, Journal of Materials Science: Materials in Electronics 32 (2021) 9675–9684.

[69] J.D. Bobić, R.M. Katiliute, M. Ivanov, M.M. Vijatović Petrović, N.I. Ilić, A.S. Džunuzović, J. Banys, B.D. Stojanović, Dielectric, ferroelectric and magnetic properties of La-doped $Bi_5Ti_3FeO_{15}$ ceramics, Journal of Materials Science: Materials in Electronics 27 (2016) 2448–2454.

[70] T. Shet, R. Bhimireddi, K.B.R. Varma, Grain size-dependent dielectric, piezoelectric and ferroelectric properties of $Sr_2Bi_4Ti_5O_{18}$ ceramics, J Mater Sci 51 (2016) 9253–9266.

[71] S. Kumar, K.B.R. Varma, Dielectric relaxation in bismuth layer-structured $BaBi_4Ti_4O_{15}$ ferroelectric ceramics, Current Applied Physics 11 (2011) 203–210.

[72] S.R. Mohapatra, B. Sahu, T. Badapanda, M.S. Pattanaik, S.D. Kaushik, A.K. Singh, Optical, dielectric relaxation and conduction study of $Bi_2Fe_4O_9$ ceramic, Journal of Materials Science: Materials in Electronics 27 (2016) 3645–3652.

[73] T. Patri, A. Ghosh, M.L.V. Mahesh, P.D. Babu, S.K. Mandal, M.N. Singh, Fortified relaxor ferroelectricity of rare earth substituted 4-layered $BaBi_{3.9}RE_{0.1}Ti_4O_{15}$ (RE = La, Pr, Nd, and Sm) Aurivillius compounds, Sci. Rep. 12 (2022).

[74] H. Zhang, H. Yan, H. Ning, M.J. Reece, M. Eriksson, Z. Shen, Y. Kan, P. Wang, The grain size effect on the properties of Aurivillius phase $Bi_{3.15}Nd_{0.85}Ti_3O_{12}$ ferroelectric ceramics, Nanotechnology 20 (2009) 385708.

[75] P. Nayak, T. Badapanda, A.K. Singh, S. Panigrahi, Possible relaxation and conduction mechanism in W6+doped $SrBi_4Ti_4O_{15}$ ceramic, Ceram Int 43 (2017) 4527–4535.

[76] F. Rehman, J.B. Li, Y.K. Dou, J.S. Zhang, Y.J. Zhao, M. Rizwan, S. Khalid, H.B. Jin, Dielectric relaxations and electrical properties of Aurivillius $Bi_{3.5}La_{0.5}Ti_2Fe_{0.5}Nb_{0.5}O12$ ceramics, J. Alloys. Compd. 654 (2016) 315–320.

[77] A.K. Thomas, K. Abraham, J. Thomas, K. V. Saban, Electrical and dielectric behaviour of $Na_{0.5}La_{0.25}Sm_{0.25}Cu_3Ti_4O_{12}$ ceramics investigated by impedance and modulus spectroscopy, Journal of Asian Ceramic Societies 5 (2017) 56–61.

[78] F. Rehman, J.B. Li, P. Ahmed, M.S. Khan, Y. Saeed, A. khan, M. Zubair, Dielectric relaxation and conduction behaviors of Aurivillius $Na_{0.5}Bi_{4.5}Ti_4O_{15}$ ceramics with Na doping, Rare Metals 40 (2021) 1247–1254.

[79] E Venkata Ramana, NV Prasad, F Figueiras, L Lajaunie, R Arenal, G Otero-Irurueta, MA Valente, The growth and improved magnetoelectric response of strain-modified Aurivillius $SrBi_{4.25}La_{0.75}Ti_4FeO_{18}$ thin films, Dalton Trans. 48 (2019) 13224.

[80] A. Faraz, T. Maity, M. Schmidt, N. Deepak, S. Roy, M.E. Pemble, R.W. Whatmore, L. Keeney, Direct visualization of magnetic-field-induced magnetoelectric switching in multiferroic Aurivillius phase thin films, Journal of the American Ceramic Society 100 (2017) 975–987.

[81] J. Paul, S. Bhardwaj, K.K. Sharma, R.K. Kotnala, R. Kumar, Room temperature multiferroic properties and magnetoelectric coupling in Sm and Ni substituted $Bi_{4-x}Sm_xTi_{3-x}Ni_xO_{12\pm\delta}$ (x = 0, 0.02, 0.05, 0.07) ceramics, J Appl Phys 115 (2014).

[82] H. Zhao, H. Kimura, Z. Cheng, M. Osada, J. Wang, X. Wang, S. Dou, Y. Liu, J. Yu, T. Matsumoto, T. Tohei, N. Shibata, Y. Ikuhara, Large magnetoelectric coupling in magnetically short-range ordered $Bi_5Ti_3FeO_{15}$ film, Sci Rep 4 (2014).

[83] T. Patri, J. Praveen Kumar, A. Ghosh, P.D. Babu, Tunable polarization with enhanced multiferroic response of W/Co co-doped $Bi_4LaFeTi_3O_{15}$ Aurivillius ceramics, J. Appl. Phys. 128 (2020).

[84] R. Ti, C. Wang, H. Wu, Y. Xu, C. Zhang, Study on the structural and magnetic properties of Fe/Co co-doped $Bi_4Ti_3O_{12}$ ceramics, Ceram. Int. 45 (2019) 7480–7487.

[85] Y. Wang, H. Wang, W. Tan, D. Huo, Magnetization reversal, critical behavior, and magnetocaloric effect in $NdMnO_3$: The role of magnetic ordering of Nd and Mn moments, J. Appl. Phys. 132 (2022).

[86] W. Bai, C. Chen, J. Yang, Y. Zhang, R. Qi, R. Huang, X. Tang, C.G. Duan, J. Chu, Dielectric behaviors of Aurivillius $Bi_5Ti_3Fe_{0.5}Cr_{0.5}O_{15}$ multiferroic polycrystals: Determining the intrinsic magnetoelectric responses by impedance spectroscopy, Sci Rep 5 (2015).

[87] T. Li, H. Wang, D. Ma, K. Li, Z. Hu, Influence of clamping effect in $BaTiO_3$ film on the magnetoelectric behavior of layered multiferroic heterostructures, Mater. Res. Bull. 115 (2019) 116–120.

[88] Y. Liu, Y. Pu, Z. Sun, Correlation between lattice distortion and magnetic and electrical properties of Fe-doped $Bi_4Ti_3O_{12}$ ceramics, Journal of Materials Science: Materials in Electronics 26 (2015) 7484–7489.